

VALIDATION OF NAVIER-STOKES COMPUTATIONS AND A TRANSITION MODEL

By Erkki Soenne, Linköping, Sweden

Presented at the XXVI OSTIV Congress, Bayreuth, Germany

ABSTRACT

Two-dimensional Navier-Stokes computations have been carried out on the FX 66-17AII-182 airfoil using the ns2d code. The computational four block structured grid was created with the Icem Mulcad mesh generator taking into account the airfoil finite thickness trailing edge. A two-layer k-ε turbulence model was employed in the computations with an empirical transition prediction model. Computations were performed at Reynolds numbers 1.5 and 3 million in 64 cases altogether. The computed lift, drag and pitching moment coefficients are compared with existing wind tunnel data.

NOTATION

c_f	local skin friction coefficient
c_{ϵ_1}	turbulence model constants
c_{μ}	turbulence model constant
C_p	pressure coefficient
ds	first cell size
f_i	damping functions
H	boundary layer shape factor
k	turbulent kinetic energy
K	factor in stretching function
l	parameter in Thwaites's method
Ma	Mach number
N	logarithm of the amplification ratio of Tollmien-Schlichting waves
N_{crit}	critical value of N
P	production term of turbulence
Re	Reynolds number based on airfoil chord
Re_{θ}	Reynolds number based on momentum thickness
Re_{inc}	critical Reynolds number
R_{yn}	Reynolds number referred to the normal distance from the wall
R_{yn}^*	critical Reynolds number
s	Streamwise coordinate
S	source term of turbulence
t	time
u_t	friction velocity
u_j	time averaged velocity component in Cartesian coordinate direction x_j
U	local velocity
U_e	external flow velocity
U_{∞}	free stream velocity
x_j	component of Cartesian coordinate
y	coordinate in boundary layer thickness direction
y_n	normal distance from the wall
Y^+	dimensionless normal distance from the wall
α	angle of attack

δ	boundary layer thickness
δ^*	displacement thickness
ϵ	dissipation rate of turbulent kinetic energy; factor in stretching function
λ	Dimensionless pressure gradient parameter
μ	Dynamic viscosity
μ_t	Turbulent eddy viscosity
ν	kinematic viscosity
ρ	density
σ_{ϵ}	Turbulence model constant
σ_k	Turbulence model constant
Θ	Momentum thickness

INTRODUCTION

Navier-Stokes computations are a new method to analyze flows around transition free airfoils. The author presented in the previous OSTIV Congress a paper with computations on FX 61-163 airfoil. The analysis contained two restrictions: the airfoil trailing edge was modeled with zero thickness and the transition locations were prescribed to match the wind tunnel experiments. The airfoil cusped trailing edge was shown to have a noticeable effect on the computed results. Because the exact trailing edge geometry of the wind tunnel model was not known, an exact comparison between the experiments and computations was not possible.

In this study, another well defined airfoil was chosen for the validation of computations. FX 66-17AII-182 airfoil was chosen because wind tunnel tests, performed in NASA low-turbulence pressure tunnel in Langley by Somers [14], were available with also a measurement on the model geometry. The wind tunnel model had a finite thickness trailing edge. This airfoil has been used on the Standard Libelle, Standard Cirrus and Salto gliders.

The modeling of a finite trailing edge thickness is usually considered to be a complication. For example in the computations of the A310 slotted airfoil (ref. [6]) the main airfoil trailing edge was modified to end in zero thickness to ease the meshing and the computations. However, there will always be the question what effect a geometry modification may have on the computed results. To avoid that kind of discussion the grid generation is performed here on the exact wind tunnel model geometry.

Another extension in the analysis is the prediction of the boundary layer transition location. In a Navier-Stokes code the laminar boundary layer is solved from the Navier-Stokes equations for laminar flow and the turbulent boundary layer using the turbulence model in question. The transition location is prescribed in the analysis. However, in many engineering applications the transition location (or zone) is not always known. A transition prediction method is needed that allows the movement of the transition location independent of the Navier-Stokes solution. Then it is possible for the transition location to move downstream into the turbulent boundary layer. The Navier-Stokes code adapts the solution accordingly and when there is no change in the location the process has converged.

In this study the transition prediction is based on computing the laminar boundary layer parameters with Thwaites's method and checking transition due to Tollmien-Schlichting instability waves with the e^N -method.

COMPUTER CODE

The utilized code ns2d of Saab Aerospace solves the two-dimensional time-dependent compressible flow Reynolds averaged Navier-Stokes equations written in conservative form. The equations are solved in a structured multiblock domain. The mean flow equations are specified in a space-centered finite volume approximation. A blending of adaptive second and fourth order artificial dissipation terms is added to the numerical scheme to damp spurious oscillations and improve convergence. The mean flow equations are integrated in time using an explicit five-step Runge-Kutta scheme. Local time steps as well as multigrid technique are available for convergence acceleration. The far field boundary velocities are corrected based on circulation, equivalent with the airfoil lift. The airfoil lift, drag and pitching moment are determined by surface integration of pressure and wall shear stress. A description of the governing equations and the ns2d code is presented by the author in reference [11].

The code is intended primarily for the analysis of commercial and military airplanes where the flows are mainly turbulent and often separated. The code has been validated in BRITE/EURAM EUROVAL and GARTEUR collaborative projects with applications such as Aerospatiale AS239 airfoil, NLR7301 flapped airfoil and Airbus A310 three element airfoil. Here a special version of the code was used where transition prediction was implemented for preliminary testing. The transition model could be started only on the fine mesh level.

TURBULENCE MODEL

Turbulence models based on two differential equations are called two-equation models; an example of which is the k - ϵ turbulence model employed in this investigation. In these models the turbulent kinetic energy k and its dissipation rate ϵ are obtained from their transport equations that have a generalized form

$$\frac{\partial}{\partial t}(\rho k) + \frac{\partial}{\partial x_j}(\rho \bar{u}_j k) = \frac{\partial}{\partial x_j} \left[\left(\mu + \frac{\mu_T}{\sigma_k} \right) \frac{\partial k}{\partial x_j} \right] + P_k - \rho \epsilon - S_k \quad (1)$$

$$\frac{\partial}{\partial t}(\rho \epsilon) + \frac{\partial}{\partial x_j}(\rho \bar{u}_j \epsilon) = \frac{\partial}{\partial x_j} \left[\left(\mu + \frac{\mu_T}{\sigma_\epsilon} \right) \frac{\partial \epsilon}{\partial x_j} \right] + \frac{\epsilon}{k} (c_{\epsilon 1} P_k - c_{\epsilon 2} f_2 \rho \epsilon) - S_\epsilon \quad (2)$$

where t is time, ρ density, μ dynamic viscosity and μ_t turbulent eddy viscosity. \bar{u}_j is the time averaged velocity com-

ponent in the Cartesian coordinate direction X_i . P denotes a production term and S a source term. Factors f are damping functions in the vicinity of a wall and σ_k , σ_ϵ and $c_{\epsilon i}$ are empirical constants. The kinetic energy and its dissipation rate can be solved for using the two equations. The turbulent eddy viscosity is obtained from the equation applicable for k - ϵ turbulence models

$$\mu_t = \rho c_\mu f_\mu \frac{k^2}{\epsilon} \quad (3)$$

where c_μ is a model constant and f_μ a damping function.

In this work the two-layer turbulence model has been used that was documented in the previous OSTIV paper [11]. However, there is a new automatic routine for the switching index, describing where to shift from the inner Wolfshtein model [16] to the standard turbulence model of Jones and Launder [8].

The method is based on the paper of Jongen and Marx [9], however without representing the boundary layer as a linear combination of the two layers. The determination of the switching index is simply based on the Reynolds number referred to the normal distance y_n from the wall

$$R_{y_n} = \frac{\sqrt{k} y_n}{\nu} \quad (4)$$

where ν is kinematic viscosity. The critical Reynolds number is chosen a value such that switching occurs in the logarithmic region of the boundary layer. In ns2d code is chosen a value

$$R_{y_n}^* = 150 \quad (5)$$

which is in the interval of 50...200, recommended by Jongen and Marx. If the Reynolds number based on the normal distance from the wall is smaller than the critical value, then the near-wall model of Wolfshtein is used, else the Jones-Launder model is employed.

Within every computational block the number of cells from the wall, corresponding to the critical Reynolds number, is computed at every streamwise station. The obtained maximum number of cells is rounded up to the nearest integer, divisible by four, in preparation for three level multigrid usage. The number of cells in the inner region is bounded by four and the maximum number of cells in the normal direction. The method has in practice shown to be robust and convenient.

TRANSITION PREDICTION

Transition is predicted in ns2d code by computing the laminar boundary layer parameters with Thwaites's method and checking transition due to Tollmien-Schlichting instability waves with the e^N -method. Thwaites's method also

gives the separation point for the laminar boundary layer. The boundary layer shape factor H and the Reynolds number based on momentum thickness Re_θ are defined

$$H = \frac{\delta^*}{\theta} \quad (6)$$

and

$$Re_\theta = \frac{\rho_e U_e \theta}{\mu_e} \quad (7)$$

where the displacement and momentum thicknesses are

$$\delta^* = \int_0^\delta \left(1 - \frac{\rho U}{\rho_e U_e}\right) dy \quad (8)$$

$$\theta = \int_0^\delta \frac{\rho}{\rho_e} \left(1 - \frac{U}{U_e}\right) \frac{U}{U_e} dy \quad (9)$$

and where U is local velocity. Subscript 'e' refers to conditions at a boundary layer external edge and δ is the boundary layer thickness.

From assumptions of uni-parametric velocity profiles, algebraic relations are obtained in Thwaites's method between Θ , H and the friction coefficient c_f , the unknowns in the von Karman momentum integral equation

$$\frac{d\theta}{ds} + (2 + H) \frac{\theta}{U_e} \frac{dU_e}{ds} = \frac{1}{2} c_f \quad (10)$$

where s is the streamwise coordinate. By introducing a dimensionless pressure gradient parameter

$$\lambda = \frac{\rho \theta^2 dU_e}{\mu ds} \quad (11)$$

the integral equation can be rewritten as (see Moran [10])

$$\frac{\rho U_e d}{\mu ds} (\theta^2) = 2[l - (2 + H)\lambda] \quad (12)$$

where

$$l = \frac{1}{2} Re_\theta c_f \quad (13)$$

Thwaites found that to an excellent approximation l and H are functions only of λ . His method is based on the notion that the RHS of equation (12) is very well approximated by

$$2[l - (2 + H)\lambda] = 0.45 - 6\lambda \quad (14)$$

This yields a first order differential equation for the momentum thickness

$$\frac{d}{ds} (\theta^2 U_e^6) = 0.45 v U_e^5 \quad (15)$$

where v is kinematic viscosity.

The velocity of an inviscid flow at stagnation point is generally analytic and can be expanded in a power series at that point. Substituting a linear approximation for the velocity into equation (15), integrating and assuming that the momentum thickness is finite at the stagnation point an expression for it is obtained

$$\theta(0) = \sqrt{\frac{0.075\mu}{\rho \left(\frac{dU_e}{ds}\right)_0}} \quad (16)$$

Then, the momentum thickness can be integrated downstream the boundary layer from equation (15). U_e is known from the pressure distribution of the Navier-Stokes solution.

The form parameter is computer derived using the correlation formulas

$$H(\lambda) = 2.088 + \frac{0.0731}{\lambda + 0.14} \quad -0.1 < \lambda < 0 \quad (17)$$

$$H(\lambda) = 2.61 - 3.75\lambda + 5.24\lambda^2 \quad 0 < \lambda < 0.1 \quad (18)$$

given by Cebeci and Bradshaw [5].

Thwaites method is not valid for separated flows. Separation is predicted to occur at $l=0$ as l is proportional to the local skin friction coefficient, see equation (13). This corresponds with values $\lambda=0.0898$ and $H=3.5$, derived from equations (17) and (18), and the integration is stopped there. If separation of the laminar boundary layer occurs before the transition, it is assumed in the code that transition takes place 2% chord downstream of the separation point.

The transition prediction, based on linear stability theory, assumes that transition will occur when the most amplified Tollmien-Schlichting waves have grown a factor e^N . Drela and Giles [7] solved the Orr-Sommerfeld equation using Falkner-Skan velocity profiles for the spatial ampli-

fication rates of a range of shape parameters and unstable frequencies. The logarithm of the amplification ratio N is calculated by integrating the local amplification rate downstream from the point of instability as

$$N = \int_{Re_{\theta c}}^{Re_{\theta}} \frac{dN}{dRe_{\theta}} dRe_{\theta} \quad (19)$$

No amplification will take place for $Re_{\theta} < Re_{\theta c}$ by setting $dN/dRe_{\theta} = 0$. The slope of the maximum amplification rate dN/dRe_{θ} is assumed to be only a function of the local shape factor H using the empirical relation

$$\frac{dN}{dRe_{\theta}} = 0.01 \left[\{ 2.4H - 3.7 + 2.5 \tanh(1.5H - 4.65) \}^2 + 0.25 \right]^{1/2} \quad (20)$$

The critical Reynolds number $Re_{\theta c}$ is expressed through the empirical formula

$$\log_{10} Re_{\theta c} = \left(\frac{1.415}{H-1} - 0.489 \right) \times \tanh \left(\frac{20.0}{H-1} - 12.9 \right) + \frac{3.295}{H-1} + 0.44 \quad (21)$$

Equation (19) is integrated downstream from the stagnation point and transition occurs when N reaches some critical value. In this work the default value $N_{crit} = 9$ has been used.

The determination of the transition location is an iterative process in the code. Using the pressure distribution, obtained from the Navier-Stokes solution, the laminar boundary layer is calculated with the Thwaites method and a new transition location with the e^N -method. The new location may be upstream or downstream of the old one and is set for the next iteration of the Navier-Stokes solution. The procedure is continued until the transition location does not change. In the ns2d code, the user can specify the number of Navier-Stokes iterations between every transition location computation. In this work a value of 100 Navier-Stokes iterations has been used.

WIND TUNNEL TESTS

The FX 66-17All-182 airfoil has been tested in the laminar flow wind tunnel at the Technical University of Stuttgart by Althaus [2] and later on in the Langley low-turbulence pressure tunnel by Somers [14]. The models in the Stuttgart tunnel were fabricated with the same methods as used in manufacturing the gliders of composite construction. Althaus [1] has made an investigation showing

that the obtained accuracy causes no penalties in airfoil performance. Thus only the nominal airfoil coordinates are reported in reference [2].

However, for the validation of CFD computations the exact geometry of the wind tunnel test model is needed. Consequently the experiments by Somers are used here because he reports the measured model geometry that was employed in the wind tunnel tests. The contours of the nominal airfoil and the wind tunnel model are shown in fig. 1.

The Langley low-turbulence pressure tunnel (ref. [15]) is a closed-throat, single return tunnel where the Reynolds number can be varied through the pressurization of the tunnel. The tunnel has a contraction ratio of 17.6 and eleven screens giving a turbulence level of approximately 0.025% with the Reynolds numbers in question. The test section is rectangular measuring 0.9 m times 2.3 m. The 0.45 m chord airfoil spanned over the test section with hydraulically actuated circular end plates providing positioning and attachment. The plates, 1.0 m in diameter, were flush with the tunnel sidewalls and rotated with the model.

The airfoil lift and pitching moment was measured through pressure integration from pressure taps on the airfoil surface. A fixed wake survey rake was cantilevered from the tunnel sidewall at the model midspan for drag measurement. There was no averaging of the possible spanwise variation of the drag due to laminar boundary layer separation bubbles. The measured aerodynamic coefficients were corrected with standard low-speed wind tunnel corrections. The corrections were approximately 1% of the measured coefficients. Transition locations were measured both with oil film visualization and listening with a stethoscope through the pressure taps.

The Langley low-turbulence pressure tunnel is one of the most famous wind tunnels where airfoil development has been performed. For example classical NACA 4, 5 and 6-series airfoils have been measured in this tunnel. However, there is not an assessment on the total accuracy of the measured aerodynamic coefficients in the report of the present wind tunnel test [14]. Also, in this test there was no boundary layer suction applied on the tunnel walls which may cause an uncertainty on the maximum lift coefficients.

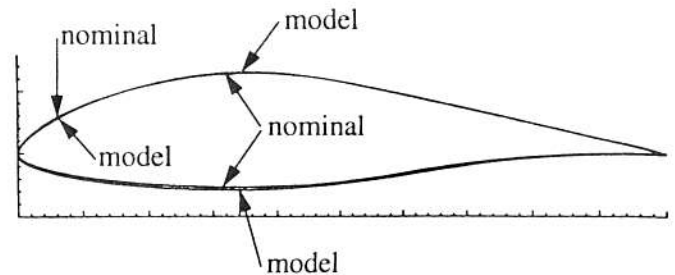


Figure 1. Contours of FX 66-17All-182 nominal airfoil and wind tunnel model [14].

MESH GENERATION

The modified C-type mesh was extended 10 chord lengths away from the airfoil. The four block mesh, created with Icem grid generator, contained altogether 30,652 nodes. The number and distribution of nodes was based on the grid variation and grid convergence studies performed by the author on another airfoil in ref. [12]. The deformation of the mesh cells was checked visually, see fig. 2.

The wind tunnel model had a finite trailing edge thickness of 0.08 percent of the airfoil chord. The geometry was accurately modeled by using 32 cells over the trailing edge thickness, see fig. 3.

In the boundary layers the stretching of the cells in the wall normal direction was increased gradually using a special function (see Blottner [3])

$$ds_j = ds_{j-1} \left(1 + \epsilon \sin \left(K \pi \frac{j-1}{j_{\max}-1} \right) \right) \quad (22)$$

where ds_j is the height of the cell j and K was selected at 0.5 to employ a quarter of a sine wave. The user specifies the first cell height, the number of cells with stretching 1.0 at the beginning of the interval, the number of cells with constant stretching at the end of the interval, the factor K and the total number of cells over the interval. The program then adjusts the factor ϵ so that the specified requirements are fulfilled.

In streamwise direction and outside the boundary layers a hyperbolic tangential stretching function was used. Within the boundary layers a maximum stretching of 1.1 was used. Outside the boundary layers a value of 1.25 was employed (with a maximum value of 1.5 allowed locally).

To ensure a sufficient resolution of the boundary layers the first cell size was based on the requirement of $y^+ = 1$ at the cell center. Using the 1/7 power velocity profile approximation for incompressible flow turbulent boundary

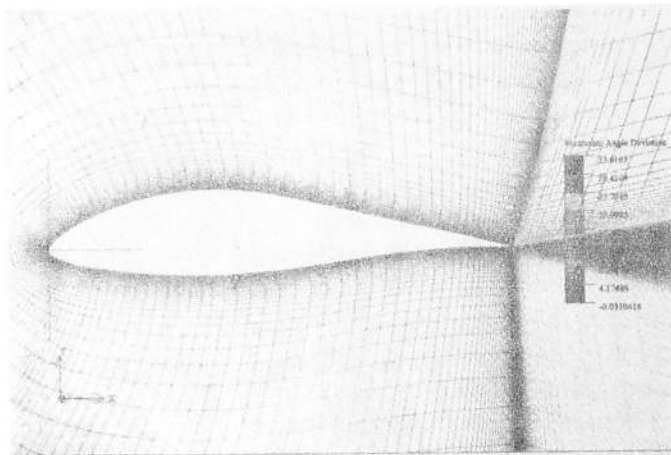


Figure 2. Distribution of maximum angle deviation on the grid of FX 66-17AII-182 airfoil.

layer over a flat plate an analytic expression was derived by the author [13] for the required cell size ds divided by the airfoil chord c

$$\frac{ds}{c} = 2 \sqrt{\frac{0.37^{1/4} \left(\frac{x}{c} \right)^{1/5}}{0.0225 Re^{9/5}}} \quad (23)$$

where x/c is the dimensionless distance from the airfoil leading edge and the Reynolds number Re is based on airfoil chord. Due to the exponent, the dimensionless distance is only a weak parameter. Because the pressure distribution on an airfoil differs from that of a flat plate it is not feasible to study the effect of the dimensionless distance but one can compute the required cell size at the trailing edge and choose a value with some margin. Expression (23), applied at the airfoil trailing edge at $x/c=1$, is depicted in fig. 4.

The first cell size was conservatively chosen as $ds=1.0 \cdot 10^{-5}$ with an airfoil chord of unity. The streamwise cell length at the trailing edge was chosen as 0.01% chord based on sensitivity studies performed by the author on another airfoil with a finite trailing edge thickness [12]. An example of the obtained y^+ values in the first cells around the airfoil is shown in fig. 5. The stagnation point on the airfoil lower surface aft of the leading edge manifests itself as a low value of y^+ . The suction peak at the leading edge shows up as a local peak value. The high values at the trailing edge are due to the chosen streamwise cell length 0.01% chord that is the first cell size aft of the finite thickness trailing edge.

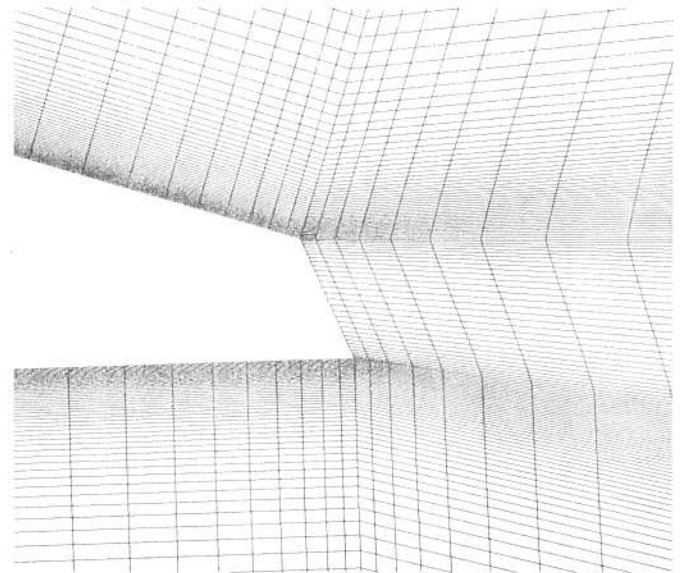


Figure 3. Close-up view of the grid at the airfoil 0.08% chord thick trailing edge.

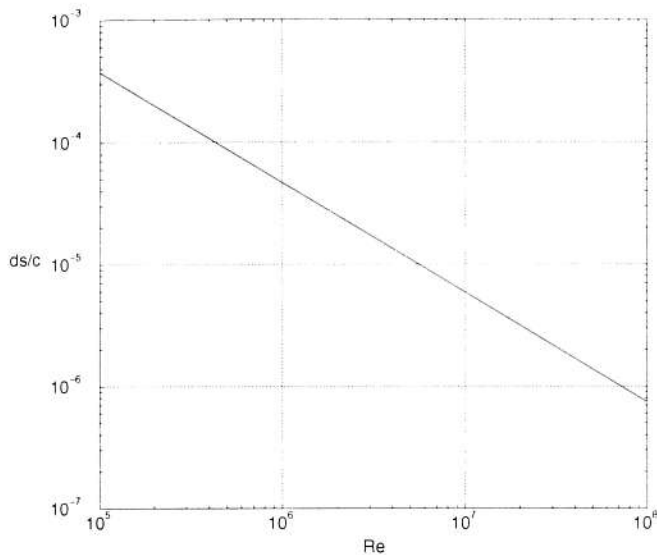


Figure 4. Maximum dimensionless first cell size as function of Reynolds number.

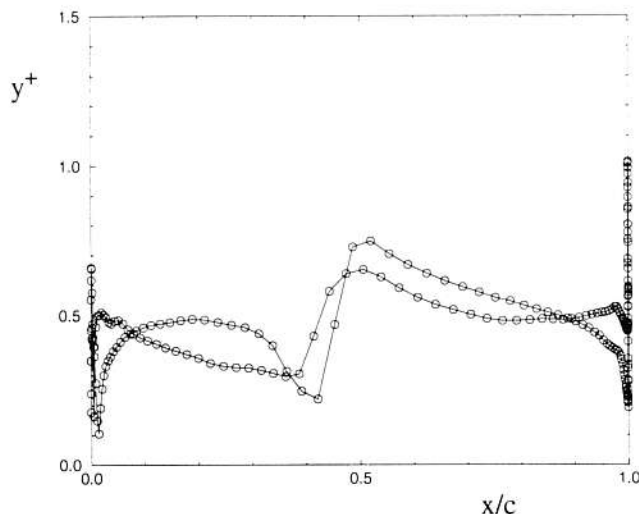


Figure 5. Distribution of y^+ in the first cell center around FX 66-17AII-182 airfoil. $\alpha=0$, $Ma=0.1$, $Re=3.0 \cdot 10^6$.

COMPUTATIONAL PROCEDURE

In this study three sets of computations were carried out:

- transition specified from the wind tunnel tests, $Re=1.5 \cdot 10^6$, $Ma=0.10$
- transition free, $Re=1.5 \cdot 10^6$, $Ma=0.10$
- transition free, $Re=3.0 \cdot 10^6$, $Ma=0.10$

The computations were started in the first set at zero angle of attack and then followed with increasing and decreasing angles of attack by using the previously obtained solution as an initial state for a new angle of attack solution. The same procedure was used for transition free computations. However, the transition prediction computations could be run only on the fine mesh level.

With the 194 MHz SGI Power Challenge processor the computing time to 20,000 work units (iterations on fine mesh level) was approximately 12 hours. An example of a convergence plot is shown in fig. 6. Beyond the angle of attack of the maximum lift coefficient according to the experiments, it was successively more difficult to obtain a steady state solution in spite of runs up to 60,000 work units. First, the drag coefficient showed a tendency for oscillation and eventually, the same was true for the lift coefficient.

The total temperature, that should be constant throughout the flow in low-speed viscous flow, was checked as a screening test. The distributions, not shown here, showed that total temperature was constant everywhere with a good accuracy.

AERODYNAMIC COEFFICIENTS

The computed lift curves, drag polars and pitching moment coefficients at Reynolds number $Re=1.5 \cdot 10^6$ are shown together with the wind tunnel test values in fig. 7.

It is seen that the computed lift curves both with the transition specified and free match the experimental results in the linear lift range. The lift curve slope is slightly higher than in the wind tunnel test. In the computations of the FX 61-163 nominal airfoil the lift exceeded the measurements in the linear lift range by approximately 0.08 and the lift curve slope was 5% higher [11]. Computations with MSES code on an airfoil, having a 1.7% chord clipped trailing edge, showed a noticeable reduction in lift. Hence it was reasoned that the uncertainty in the airfoil trailing edge contour could be the cause for the difference between the ns2d computations and experiments. This is confirmed by the good matching of the computational and experimental values on the present airfoil with an exact definition of the airfoil contour.

There is also experimental evidence that small geometrical changes at the airfoil trailing edge, such as wedges and Gurney flaps, have large effect on airfoil lift. Bloy et al [4] have among aforementioned devices also tested a 2% chord 45° flap made of a thin sheet attached on the model lower surface. The increase of the lift coefficient on the model wing, with an aspect ratio of 5, was approximately 0.3 corresponding a two-dimensional value of 0.42.

In the vicinity of the angle attack $\alpha=9.5^\circ$, that corresponds to the maximum lift coefficient, the computed curves try to follow the experimental curve. However, only a local kink is created and then the computed curves continue upwards without establishing a maximum lift coefficient within the range of angle of attack values employed in the computations. There is an uncertainty in the measured maximum lift coefficient because there was no boundary layer suction on the tunnel walls to guarantee that the flow stays two-dimensional at high lift. However, the computed curves continue unreasonably high without a stall.

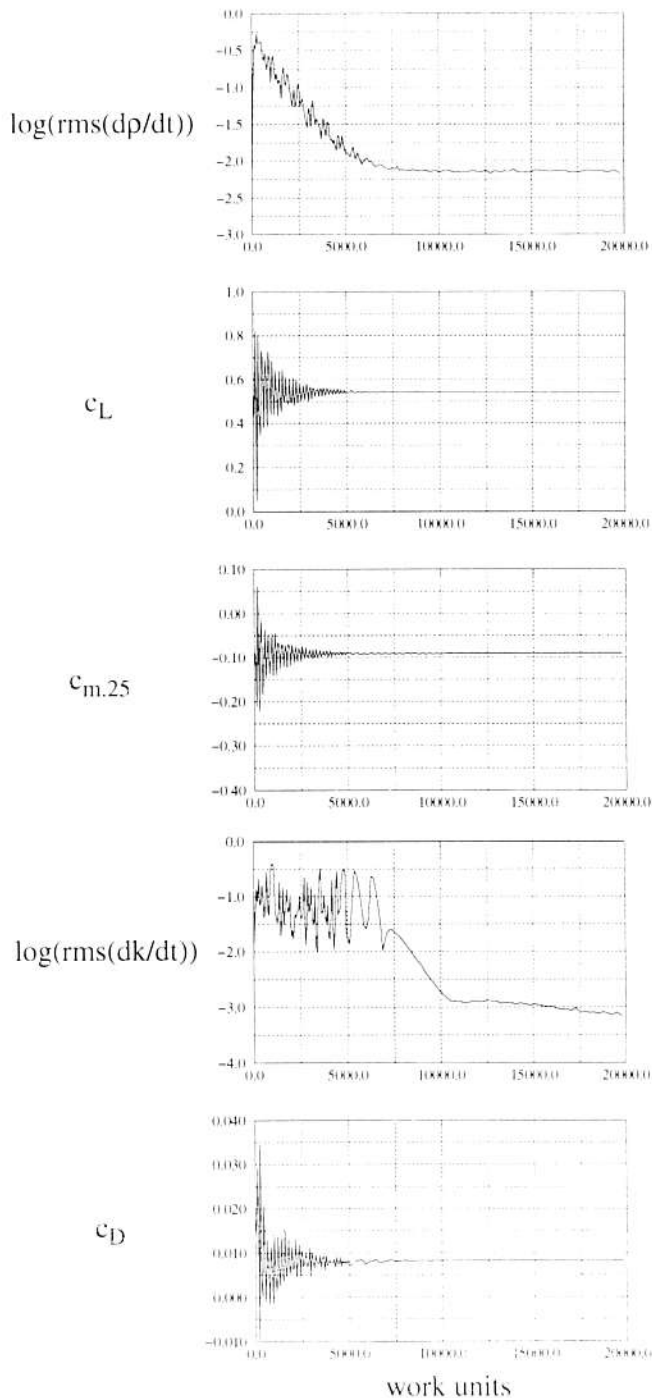


Figure 6. Convergence history on FX 66-17All-182 airfoil with transition free, $\alpha=1^\circ$, $Ma=0.1$, $Re=1.5 \cdot 10^6$. Two-layer turbulence model of *ns2d* code.

With regards to the pitching moment coefficient, the computed values are almost identical with the experimental results up to the angle of attack $\alpha=8^\circ$, where the measured and computed lift coefficients start to deviate. In the computed results of the FX 61-163 nominal airfoil there was a shift of 0.02 in the pitching moment coefficient compared with the wind tunnel test results. Obviously an

accurate definition of the airfoil trailing edge contour is also necessary for a correct pitching moment.

The computed drag polars match quite well to the measurements. Even outside the lower end of the laminar bucket the computations follow the trend of increasing drag as obtained in the experiments. At the upper end of the bucket there is only one experimental value showing drag increase. Also, the computations follow quite nicely the measurements and then show a large drag increase with increasing lift as expected. The accuracy on drag prediction is approximately the same or slightly better than on the FX 61-163 nominal airfoil.

At Reynolds number $3.0 \cdot 10^6$ only the transition model was employed as transition locations were not measured in the experiments. The computed results are collected into fig. 8 together with the experimental values.

The lift coefficient shows the same characteristics as at the lower Reynolds number with good matching in the linear lift region but failing to establish a maximum lift coefficient. The computed pitching moment coefficient agrees well with the measured values in the linear lift range. The computed drag polar matches the form of the experimental polar even outside the laminar drag bucket quite well.

DISTRIBUTIONS

The Mach number distribution and streamlines around the airfoil at angle of attack $\alpha=0^\circ$ are shown in fig. 9. It is seen in the figure that the solution is smooth with the streamlines forming a small wake area with two counter rotating vortices aft of the trailing edge. Then the streamlines continue smoothly downstream.

At 9.18° angle of attack where the computed lift curve showed a kink, the streamlines are still attached to the airfoil upper surface without a flow separation, see fig. 10. The wake aft of the trailing edge was unsteady with the streamlines leaving the trailing edge either on the upper or lower corner, see figures 10 and 11. The lift coefficient oscillated during the iterations between 1.40 and 1.41.

The pressure coefficient distributions for the two angle of attack cases are also shown in figures 9 and 10. At zero angle of attack the computed distribution agrees with the experimental curve. There is a small difference on the airfoil upper surface at 50% chord where the wind tunnel test indicates a laminar separation bubble that is not reproduced in the computation. There is also a slight difference in results on the airfoil lower surface at the 15% chord region.

At 9.18° angle of attack the computed pressure distribution also agrees with the experimental distribution. There is no separation bubble on the airfoil upper surface. Furthermore, there is no sign of incipient trailing edge separation in the form of a pressure plateau at the airfoil trailing edge region. On the airfoil lower surface aft of the leading edge the experimental and computed distributions match well. The straight line presentations differ only due to the large spacing of the experimental points. On the airfoil upper surface the computed suction

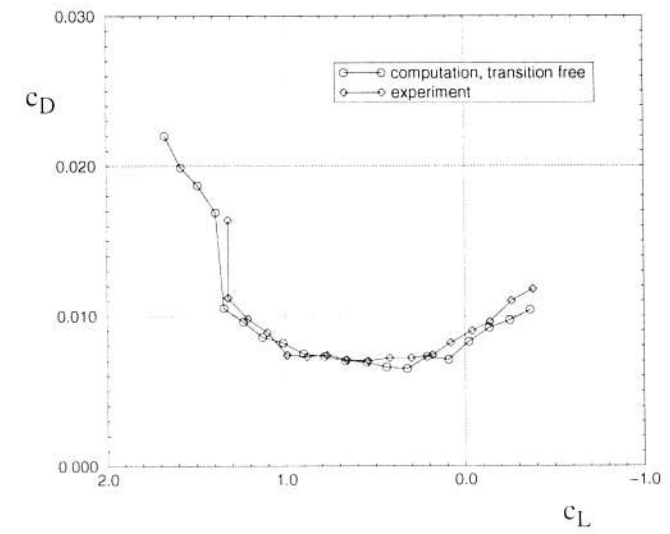
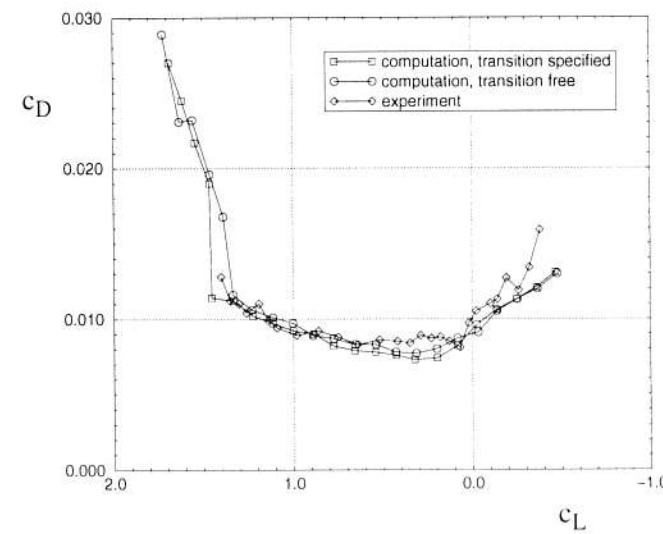
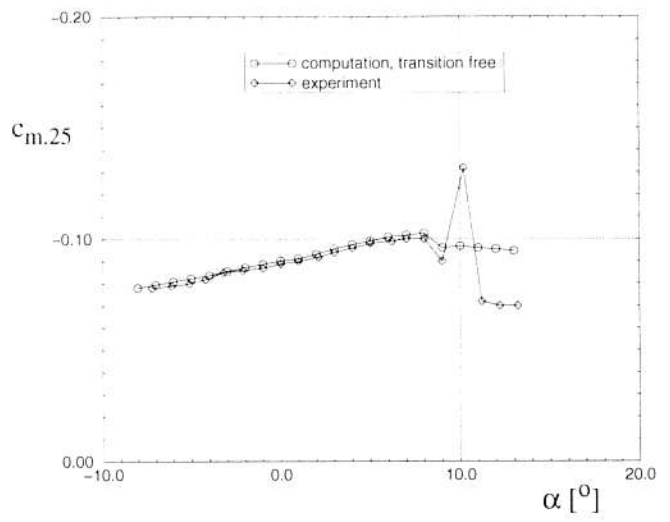
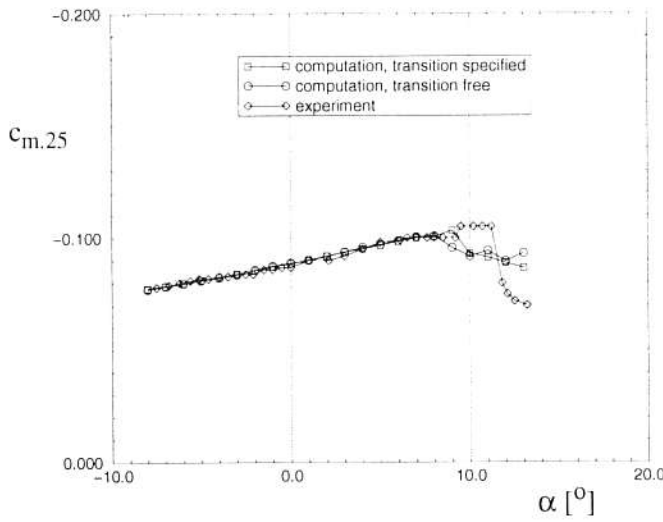
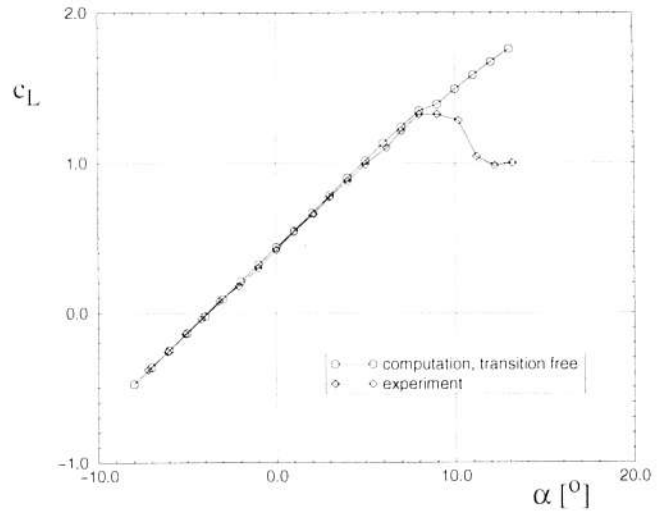
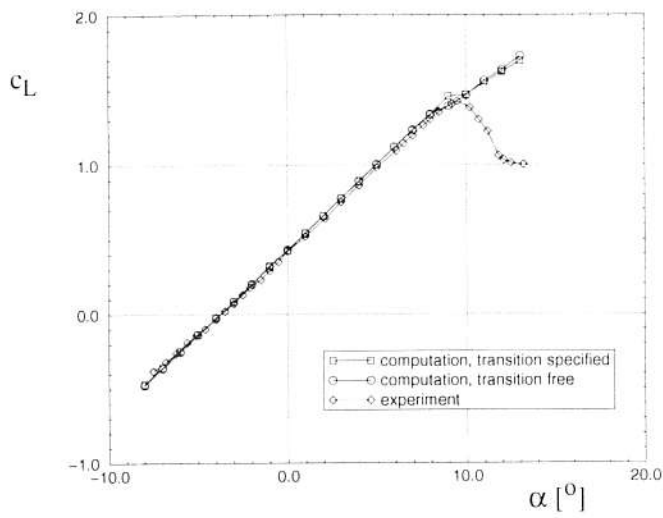


Figure 7. Lift, drag and pitching moment coefficients Figure 8. Lift, drag and pitching moment coefficients of FX 66-17AII-182 airfoil at $Ma=0.1$, $Re=1.5 \times 10^6$.

Figure 8. Lift, drag and pitching moment coefficients of FX 66-17AII-182 airfoil at $Ma=0.1$, $Re=3.0 \times 10^6$.

peak $C_p = -2.94$ somewhat exceeds the experimental value of $C_p = -2.62$.

At even higher angles of attack the experimental results

show a pressure plateau that successively expands forward from the trailing edge reaching 45% chord at an angle of attack at 12.14° . The computations showed no

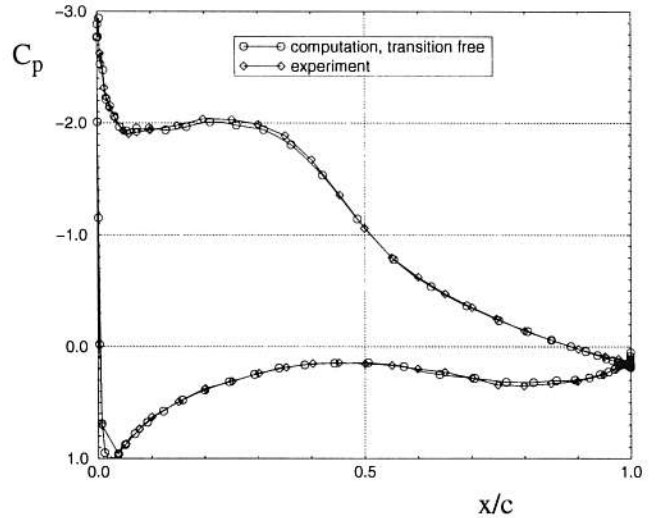
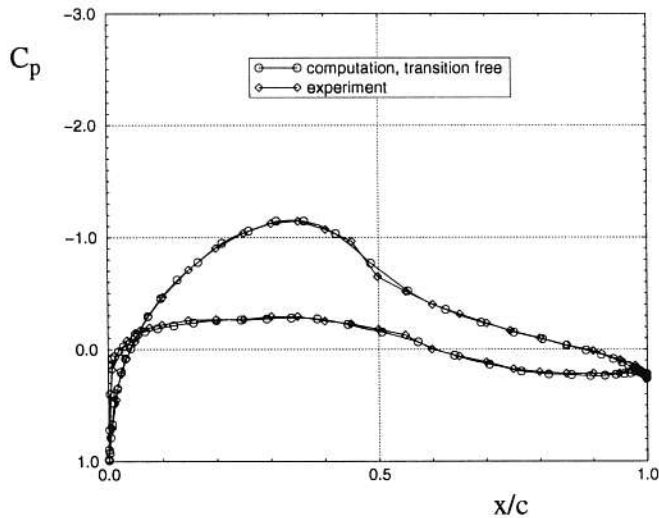
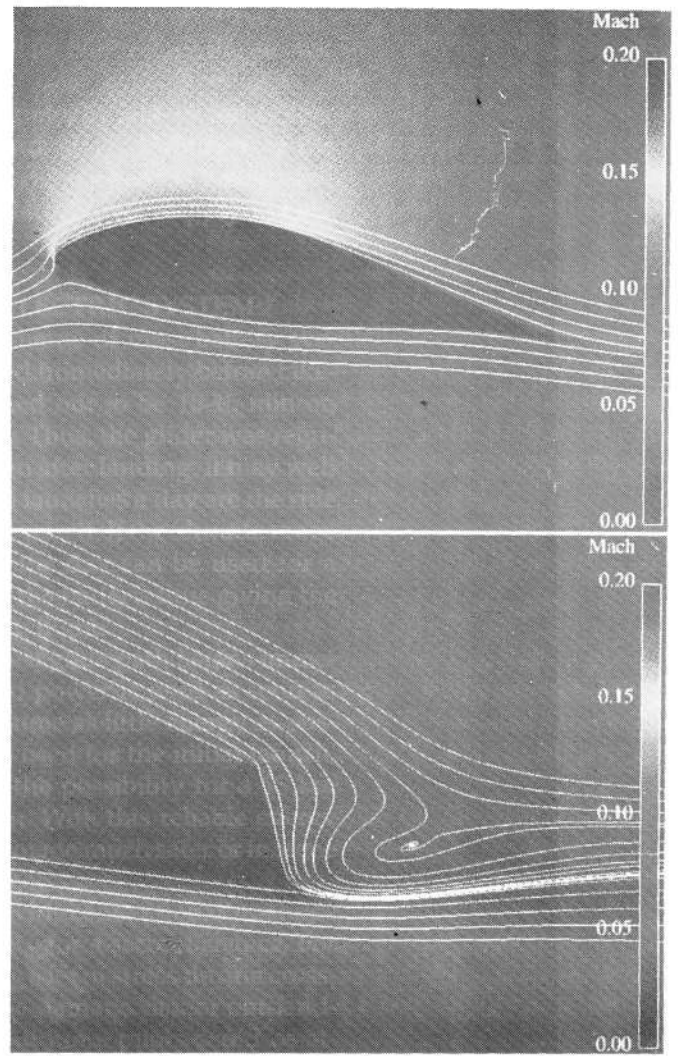
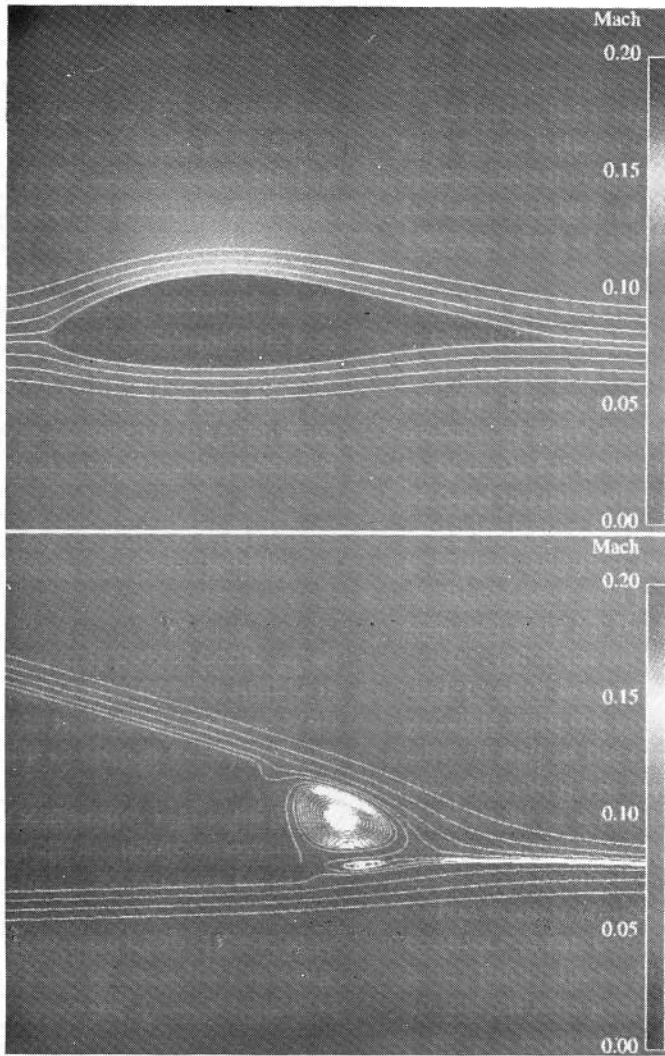


Figure 9. Computed distributions of Mach number, streamlines and pressure coefficient transition free at 20000 iterations around FX 66-17AII-182 airfoil and trailing edge. $\alpha=0^\circ$, $Ma=0.1$, $Re=1.5 \cdot 10^6$. Two-layer turbulence model of ns2d code.

Figure 10. Computed distributions of Mach number, streamlines and pressure coefficient transition free at 20000 iterations around FX 66-17AII-182 airfoil and trailing edge. $\alpha=9.18^\circ$, $Ma=0.1$, $Re=1.5 \cdot 10^6$. Two-layer turbulence model of ns2d code.

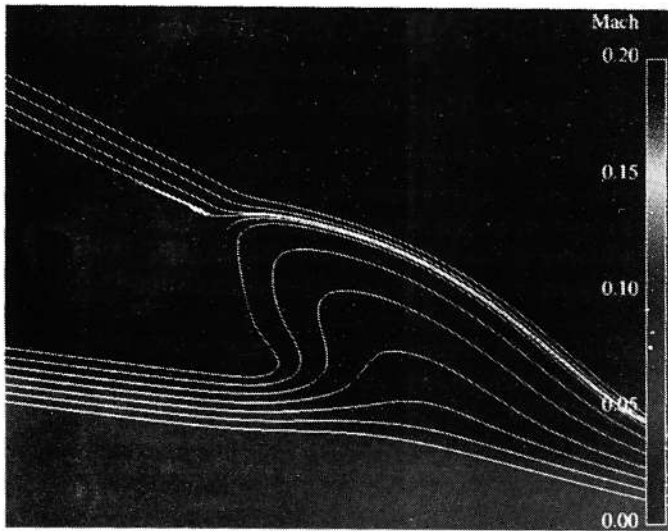


Figure 11. Computed distributions of Mach number, and streamlines transition free at 40000 iterations around FX 66-17AII-182 airfoil trailing edge. $\alpha=9.18^\circ$, $Ma=0.1$, $Re=1.5 \cdot 10^6$. Two-layer turbulence model of ns2d code.

such plateau beyond 9° angle of attack, which is the reason for excessively high lift coefficient values.

CONCLUSIONS

Computations with the Navier-Stokes program ns2d were performed with two-layer turbulence model on the FX 66-17AII-182 airfoil by modeling accurately the measured wind tunnel model geometry particularly at the finite thickness trailing edge. The lift, pitching moment and drag coefficients matched well the experiments in the linear lift range thus demonstrating the need for accurate meshing.

Test runs with the two-layer turbulence model and transition prediction routine, based on Thwaites's method on laminar boundary layer computation and amplification of Tollmien-Schlichting waves, showed the method to be robust and convenient to use. The transition prediction method gave transition locations close to the wind tunnel tests which showed in the computed drag coefficients, (computed with transition specified and free) to be close to each other.

Airfoil maximum lift coefficient was not found in the computations as there was no flow separation on airfoil upper surface within the range of investigated angles of attack. The reason for this is phenomena probably turbulence resulting from the model used. Evidently there is a need for future research in this field.

REFERENCES

- [1] Althaus D., Effects on the Polar Due to Changes or Disturbances to the Contour of the Wing Profile, Technical Soaring, Volume X, No. 1, p. 2....9.
- [2] Althaus D., Stuttgarter Profilkatalog I, Insitut für Aerodynamik und Gasdynamik der Universität Stuttgart, 1972, 386 p.
- [3] Blottner F. G., Verification of Navier-Stokes Code for Solving the Hypersonic Blunt Body Problem, Proc. Fourth Symp. on Num. and Phys. Aspects of Aerodynamic Flows, 1989.
- [4] Bloy A. W., Tsioumanis N., Mellor N. T., Enhanced Aerofoil Performance Using Small Trailing-Edge Flaps, Engineering Note, Journal of Aircraft, Vol. 34, No. 4, July-August 1997, pp. 569-571.
- [5] Cebeci T., Bradshaw P., Momentum Transfer in Boundary Layers, McGraw-HilWemispehere, Washington D.C., 1977.
- [6] de Cock K. M. J., Lindblad I., 2D Maximum lift prediction for the 59 percent span wing section of the A310 aircraft, High Lift Aerodynamics, phase IV, Garteurm-098-**, AG 25, March 23 1998, 174 p.
- [7] Drela M., Giles M. B., Viscous-Inviscid Analysis of Transonic and Low Reynolds Number Airfoils, AIAA Journal, Vol. 25, No. 10, October 1987.
- [8] Jones W.P., Launder B.E., The Prediction of Laminarization with a Two-Equation Model of Turbulence, Int. J. Heat and Mass Transfer, 15, 1972, p. 301-314.
- [9] Jongen T. Marx Y.P., Design of an Unconditionally Stable, Positive Scheme for the K-e and Two-layer Turbulence Models, Computers & Fluids Vol. 26, No. 5, 1997, pp. 469-487
- [10] Moran J., An Introduction to Theoretical and Computational Aerodynamics, John Wiley ~ Sons, 1984, 464 p.
- [11] Soinnie E., Navier-Stokes Computations on a Laminar Airfoil, XXV OSTIV Congress, Saint-Auban, France, 26 p.
- [12] Soinnie E., Validation of CFD Computations on Control Surfaces, Royal Institute of Technology, Department of Aeronautics Report No, 98-15, 1998, 83 p.
- [13] Soinnie E., Validation of Navier-Stokes Computations and a Transition Model, Royal Institute of Technology, Department of Aeronautics Report No, 99-15, to be published.
- [14] Somers D. M., Experimental and Theoretical LowSpeed Aerodynamic Characteristics of a Wortmann Airfoil as Manufactured on a Fiberglass Sailplane, NASA TN D-8324, 1977, 48 p.
- [15] von Doenhoff A. E., Abbott F. T., The Langley Two-Dimensional Low-Turbulence Pressure Tunnel, NACA Technical Note 1283, 1947, 64 p.
- [16] Wolfshtein M., The Velocity and Temperature Distribution in One-Dimensional Flow with Turbulence augmentation and Pressure Gradient, Int. J. Mass and Heat Transfer, 12, 1969, p. 301...318.